IEEE Access
Multidisciplinary | Rapid Review | Open Access Journal

Received 3 May 2024, accepted 24 May 2024, date of publication 30 May 2024, date of current version 10 June 2024.

Digital Object Identifier 10.1109/ACCESS.2024.3407365

RESEARCH ARTICLE

Chemical Foaming of Carbon Fiber-Polylactic Acid (CF-PLA) Porous Structures and Their Feasibility as EMI Shields in the X-Band

VALERIA MARROCCO[1], ROSSELLA SURACE[1], GIOVANNA CALÒ[2], (Member, IEEE), ELISABETTA BRANDONISIO[1], ILARIA MARASCO[2], FRANCESCA FILOGRANO[2], AND IRENE FASSI[3]

[1]Institute of Intelligent Industrial Technologies and Systems for Advanced Manufacturing (STIIMA), National Research Council of Italy (CNR), 70124 Bari, Italy
[2]Department of Electric and Information Engineering, Politecnico di Bari, 70125 Bari, Italy
[3]Institute of Intelligent Industrial Technologies and Systems for Advanced Manufacturing (STIIMA), National Research Council of Italy (CNR), 20133 Milan, Italy

Corresponding author: Valeria Marrocco (valeria.marrocco@stiima.cnr.it)

This work was supported in part by the Made in Italy—Circular and Sustainable (MICS) Extended Partnership through European Union NextGenerationEU Piano Nazionale di Ripresa e Resilienza (PNRR)—Missione 4 Componente 2, Investimento 1.3-D.D.1551.11-10-2022, under Grant PE00000004; and in part by the Programma Regionale RIPARTI POC PUGLIA FESR/FSE 2014/2020–ManuReFoam under Grant 49894278."

ABSTRACT The massive increase in telecommunications infrastructure and devices has recently exacerbated the necessity of developing advanced electromagnetic interference (EMI) shielding solutions. Porous structures based on conductive polymer composites (CPCs) are currently promoted as feasible options for this task. In this scenario, the chemical foaming process shows suitability for easily fabricating CPC foams with closed cells and variable porosity. Nonetheless, the process and the products have not yet been fully explored in the literature for EMI shielding purposes. Hence, this work proposes the fabrication of foams made of polylactic acid with 10wf% carbon fiber (CF-PLA) via chemical foaming. After the process assessment, the morphological and dielectric characterizations of the samples were discussed in the function of the process parameters. The results show that chemical blowing agent (CBA) weight fraction % and temperature were key in obtaining target structural and dielectric requirements enabling EMI shielding. Numerical analyses on CF-PLA foams, modeled according to morphological outcomes, were performed via the integral finite difference time domain (IFDTD) method. The obtained Scattering Parameters and shielding effectiveness (SE), between 0.5 and 12 GHz, highlighted that when foam relative density and air pore density are simultaneously high, the shielding is mainly accomplished through absorption (SE_A = 20dB) while reflection is minimized (SE_R = 2dB). Scattering Parameters and SE were also measured in the X-band showing good agreement with the numerical findings; indeed, CF-PLA foams with higher relative density and air cell density exhibited a reduction of SE_R (3dB) and a SE_A with maxima up to 30dB.

INDEX TERMS Chemical foaming process, EMI-shielding, carbon fiber polylactic acid, foam, morphology, relative permittivity, electromagnetic field absorption, shielding effectiveness.

I. INTRODUCTION

Society's lifestyle currently relies on faster telecommunications (TLC), which includes the 5G standard [1], [2] and digital support for the Internet of Things (IoT). Such a massive increase in infrastructure and devices leads to coping with electromagnetic interference (EMI) issues and EM pollution. EMI can be tackled through shielding, usually enabled by metal-based structures [3]. However, metal shields have the drawback of contributing to the EM pollution induced by secondary reflected waves. For these reasons, the research community has been exploring new

The associate editor coordinating the review of this manuscript and approving it for publication was Mohamed Kheir.

EMI shielding solutions, focusing especially on structures capable of enhancing wave absorption rather than reflection and providing, at the same time, ease of processability. In this regard, porous/cellular structures [3], [4], [5] have been proposed as suitable candidates, as they offer the opportunity to tune the porosity appropriately by implementing reticular and periodic arrangements of air pores/cells (electromagnetic band gap-like) or a random distribution, i.e., foams.

Conductive polymer composites (CPCs) have recently been examined to realize such reticular and random porous structures. CPCs are obtained by combining thermoplastic matrixes with a specific percentage of nanofillers (carbon fibers or nanoparticles, Carbon NanoTubes- CNT, graphene sheets, reduced Graphene Oxide-rGO, MXene, nanoparticles of Ag, Cu, Ni, etc.) or ferroelectric materials. Therefore, when CPCs are exploited to fabricate porous/cellular structures, the EM wave absorption mechanism can be enhanced through the interaction of EM radiation with the electroconductive lossy material. Additionally, the air pores/cells allow for the EM field entrapment attained by the internal multiple scattering, thus further improving the EMI Shielding Effectiveness (SE) [6], [7], [8], [9], [10], [11], [12], [13], [14], [15], [16], [17].

Polylactic acid (PLA) filled with conductive carbon fibers or nanoparticles displays outstanding versatility and processability when designing and manufacturing microwave absorbers. Numerous studies, mainly focused on periodically arranged porous geometries or multilayers, have been reported in the recent literature [18], [19], [20], [21], [22], [23]. Bregman et al. [18] realized periodic porous structures with different aspect ratios made of PLA with graphene nanoplatelet (xGNP) and fabricated via CNC milling. Varying the nanoplatelet filling percentage and radius of the air pores, results showed that reflection loss increased by as much as 13 dB, thus leading to SE optimization. Differently, Shi et al. [19] developed a multifunctional filament of PLA with graphene nanosheets (GNs) (9.08 vol%), then used to fabricate structures with controlled variable porosity, characterized by a SE of 34.9 dB in the X-band. In this case, the authors used the fused filament fabrication (FFF) technology, which allowed them to implement variable deposition patterns and consequently tailor the structure permittivity. With the same 3D printing technology, Lv et al. [20] observed that, for fabricating a controllable porous structure, two process parameters, i.e., infill and the deposition pattern (triangle, square, and honeycomb), can be adjusted appropriately to favor the EM waves capturing and improving final SE values. Laur et al. in [21] reported a case study where a 3D printed periodic porous structure, composed of a multiscale honeycomb configuration glued on a metallic plate, reached a superior adsorption level (22.9 dB) over a wide frequency range (2-18 GHz). Similarly, 3D printed sandwiched structures, such as a PLA substrate/ PLA honeycomb/PLA substrate [22] and a PLA substrate/polyvinylidene fluoride (PVFD) with CNT/PLA substrate [23], were studied for EMI shielding purposes at 2.4 GHz, X, and Ku bands, respectively.

When using randomly distributed porous structures, i.e., foams [24], [25] for EMI shielding applications, closed or partially open cells with small sizes and high density are recommended. In these cases, technologies based on foaming, such as batch foaming, foam extrusion, foam injection molding, and bead foaming [15], [26], [27], [28], [29], [30], [31] have been investigated. Physical foaming involving CO_2 in supercritical conditions [27], [28], and injection molding [29], [30] have been considered to attain cell type and density targets. In particular, supercritical CO_2-based foaming was used to fabricate expanded PLA (EPLA) foam with a CNT content of 2.68 wt.%. The EPLA was characterized by a high expansion ratio and cell density, excellent tensile and compressive strengths, an electrical conductivity of 0.12 S/m, and a SE of 99% in the X-band [28]. Wang et al. realized various PLA-based foams for EMI shielding by experimenting with different methods. In [29], PLA/graphite nanocomposite foams, with improved mechanical and dielectric characteristics, were fabricated through continuous foam injection molding, whereas batch foaming combined with solvent casting and steam-chest molding was utilized to obtain PLA/MWCNT foams [30]. Differently, Frackowiak et al. [31] reported a study on microporous structures for EMI shielding in the frequency range 100 kHz-1MHz, made of PLA with carbon fibers and carbon black, and realized by chemical foaming. The results showed that the foaming process improved the foams' permittivity and, consequently, the SE. However, the authors also observed that lower carbon fiber or carbon black filler percentage contents would have been preferred to accomplish higher SE.

Except for this latest study, the literature lacks a deeper investigation of the chemical foaming for fabricating random porous structures characterized by closed cells which can be used as EMI shields in the microwave range. Hence, the present article first proposes a detailed assessment of the chemical foaming process for realizing carbon-fiber-PLA (CF-PLA) foam samples. To assess the process, a design of experiment on two levels was implemented by varying the process parameters, i.e., the weight fraction of the blowing agent, foaming time, and temperature. The morphology and dielectric characteristics of the produced 8 samples were examined in the function of the process parameters. Subsequently, the Scattering parameters and SE are first predicted by numerical analyses, performed by the integral finite difference time domain (IFDTD) method, and then measured in the X-band by using a WR90 waveguide connected to a Vector Network Analyzer (VNA).

The paper is organized as follows: Section II describes the chemical foaming process and samples' characterization. Section III reports numerical results obtained via the IFDTD method applied to the foam modeled on morphological outcomes. Results concerning the scattering parameters S_{11}

and S_{21} and SE measurements in the X-band are detailed in Section IV and compared to numerical findings. Finally, conclusions are summarized in Section V.

II. CHEMICAL FOAMING PROCESS OF CF-PLA FOAMS

The chemical foaming process activates the exothermal expansion of a polymer matrix through the use of a chemical blowing agent (CBA); the CBA must be capable of reaching its decomposition temperature within the same range as the melting temperature of the polymeric blend.

Initially, the polymer pellet is mixed with the CBA; then, the mixture is placed in a silicon mold opened to the top and located in a pre-heated electric furnace (Memmert Excellent 400), where the increasing temperature starts the process.

The chemical foaming comprises three phases: cell nucleation, growth, and stabilization. During cell nucleation, the polymer/gas biphasic structure is formed due to the CBA decomposition, which produces a gas (CO_2) into the molten polymer and enables cell growth. In this heating phase, the main criticality is the liquid state of the foam, which is typically thermodynamically unstable and affected significantly by temperature fluctuations. Hence, careful control of heating conditions is essential to obtaining high-quality foams, thus reducing the risk of coalescence among cells and the consequent increase in the cell's diameter and decrease in cell number. When the foam has fully formed and filled the mold, fast cooling by air quenching (or water) must be applied to stabilize the structure (cell stabilization) and prevent the foam's cells from collapsing.

In the present study, the selected polymer matrix is the CF-PLA by Proto-pasta [32], characterized by a content of 10% of milled carbon fiber having a maximum particle size of 0.15 mm; its melting temperature is approximately 155°C, its density is 1.3 g/cm^3, and its volume flow-rate is 2-4 mm^3/s. The chosen CBA exothermic agent is the AzoDiCarbonamide - ADC by Acros Organics (with purity of 97%).

TABLE 1. Experimental factors and levels.

Factor	Low level	High level
ADC fraction (%)	1	2
Temperature (°C)	190	210
Time (min)	90	120

Table 1 reports the process parameters (ADC fraction, foaming temperature, and foaming time) selected for the experimental plan. Based on previous experimentation, screening tests, and literature, the recommended ADC fraction is 1-2 wt%. For the experiments, a two-level full-factorial design, comprising two levels of temperatures at standard atmosphere, 190°C and 210°C, foaming time, 90 and 120 min, and ADC fraction, 1% and 2%, are considered, ending in a total of 8 samples realized in a random sequence.

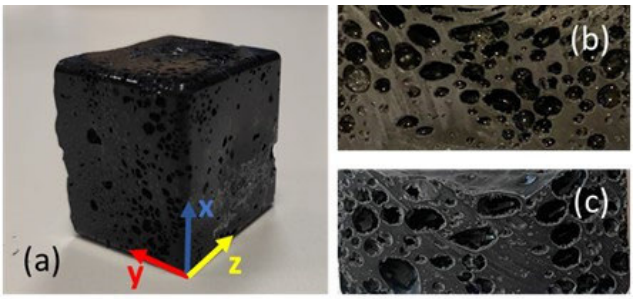

FIGURE 1. (a) Foamed sample of CF-PLA and (b-c) longitudinal sections of the foam.

A. CF- PLA-BASED FOAMS' MORPHOLOGICAL CHARACTERIZATION

Fig. 1 shows one of the foamed samples made of CF-PLA with the magnification of the longitudinal section obtained after cutting the sample with a diamond saw (Buehler Isomet).

The foam quality and characterization were first assessed by evaluating their volume after expansion, relative density, and foam morphology. The volume after the expansion was determined by measuring sample dimensions with a digital caliper, whereas the relative density was obtained by calculating the ratio of foam density and base material density (CF-PLA matrix). Table 2 reports the measured volume generated by expansion, the relative density, and the thickness of the non-foamed layer, where present. Actually, it can be observed that this layer is found for samples from 4 to 8, which have been processed at higher foam temperature and/or with higher ADC weight fraction %.

TABLE 2. Volume after expansion and relative density in function of the process parameters.

Sample	ADC weight fraction (%)	Foaming temperature (°C)	Foaming time (min)	Volume (cm^3)	Relative Density	Non-foamed layer thickness (mm)
1	1	190	90	18.249	0.340	0
2	1	190	120	18.301	0.338	0
3	2	190	90	17.911	0.344	0
4	2	190	120	15.732	0.394	4.332
5	1	210	90	19.267	0.319	4.450
6	1	210	120	19.613	0.313	4.661
7	2	210	90	18.342	0.335	4.231
8	2	210	120	18.352	0.335	3.469

Foaming with excessive ADC quantity is neither desirable nor economical and can yield a nonuniform structure. In this viewpoint, Matuana et al. [33] reported that increasing the agent content in the extrusion foaming of PLA initially enhances foams' air fraction and cell density. However, when the content is further increased (until 2%), a volume decrease is observed after reaching a maximum value, as in the present case. Indeed, higher blowing agent content may promote massive cell growth and a consequent breakage of the thin walls separating cells, which originates cell coalescence. Moreover, during solidification, due to gravity, the molten material can drain through the cell membranes, thus giving place to a non-foamed polymer layer at the bottom. Notwithstanding, such

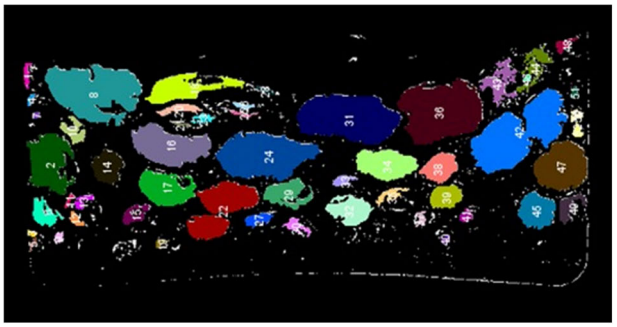

FIGURE 2. Visual acquisition of foamed sample via ImageJ software.

effects result in foams featuring a relevant material density gradient.

Visual analysis and post-processing were carried out on the samples' 2D cross-sections to evaluate the foam morphology and obtain cell density (i.e., the number of cells for the surface unit), cell dimensions, and cell circularity. For this study, the images were acquired by a 3D optical profilometer (Sensofar S Neox), and the image post-processing was performed via ImageJ software, which retrieved the cell number per area and the cell dimension.

Differently, the cell circularity was calculated via the ''circularity parameter'' C, expressed as [34]:

$$C = 4\pi A/P^2 \tag{1}$$

where A and P are the cell' area and perimeter, respectively; clearly, when C = 1, air cells are perfectly circular.

TABLE 3. Results for cell density, the median of the cell area distribution, and circularity parameter (process parameters of samples 1-8 are the same as referred in table 2).

Sample	Cell density (cells/cm^2)	Cell area distribution median (mm^2)	Circularity parameter
1	176.67	0.51	0.511
2	115.69	0.72	0.472
3	142.32	0.47	0.625
4	135.63	0.23	0.403
5	98.66	0.52	0.325
6	89.17	0.45	0.331
7	154.36	0.33	0.363
8	100.68	0.36	0.368

Table 3 summarizes the morphological results. As inferred from the data, each sample's cell density varies dramatically. Regarding cell area distribution, its representation via the median [35] has been preferred instead of average and standard deviation, as it provides more immediate information about cell dimensions. For clarity's sake, Fig. 3 reports the cell area distribution and median values related to samples 2 and 8, which have the same number of larger cells (30) but very different cell dimensions (0-1.3 mm^2 for samples 2 and 0-0.7 mm^2 for sample 8). This characteristic is promptly available by looking at the median values: sample 2 has higher median values (0.72) than sample 8 (0.36). Finally, the

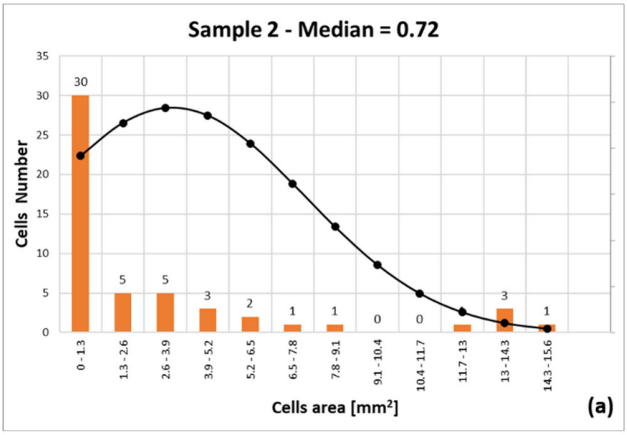

FIGURE 3. The median of the cell area distribution for (a) sample 2 and (b) sample 8.

inspection of the circularity parameter witnessed an elliptical shape of the air cells.

Usually, a well-dispersed nano-filler is expected to enhance the melt strength of the polymer because of high particle interaction, which can result in efficient stabilization of the cell structure during cell growth. Nonetheless, the PLA was demonstrated to have poor melt strength, making the production of PLA foams with superior cell morphology quite cumbersome [36]. Nevertheless, considering the final purpose of the structures, the superior cell morphology might not necessarily be desirable. In fact, higher relative density and reduced air cell dimensions are prerequisites for allowing gradient cell distribution, which is required to accomplish minimized EM wave reflection and increased absorption.

From this perspective, we evaluated how process parameters impact the relative density, the cell density, the cell area distribution, and the circularity of CF-PLA foams (Fig. 4). It can be noticed that a higher relative density (Fig. 4a) and cell density (Fig. 4b), with reduced cell area (Fig 4c) can be obtained by increasing ADC%, and decreasing the temperature. Nonetheless, reaching higher circularity (Fig. 4d) implies a reduction of ADC%, temperature, and foaming time. Therefore, the ADC% value must be

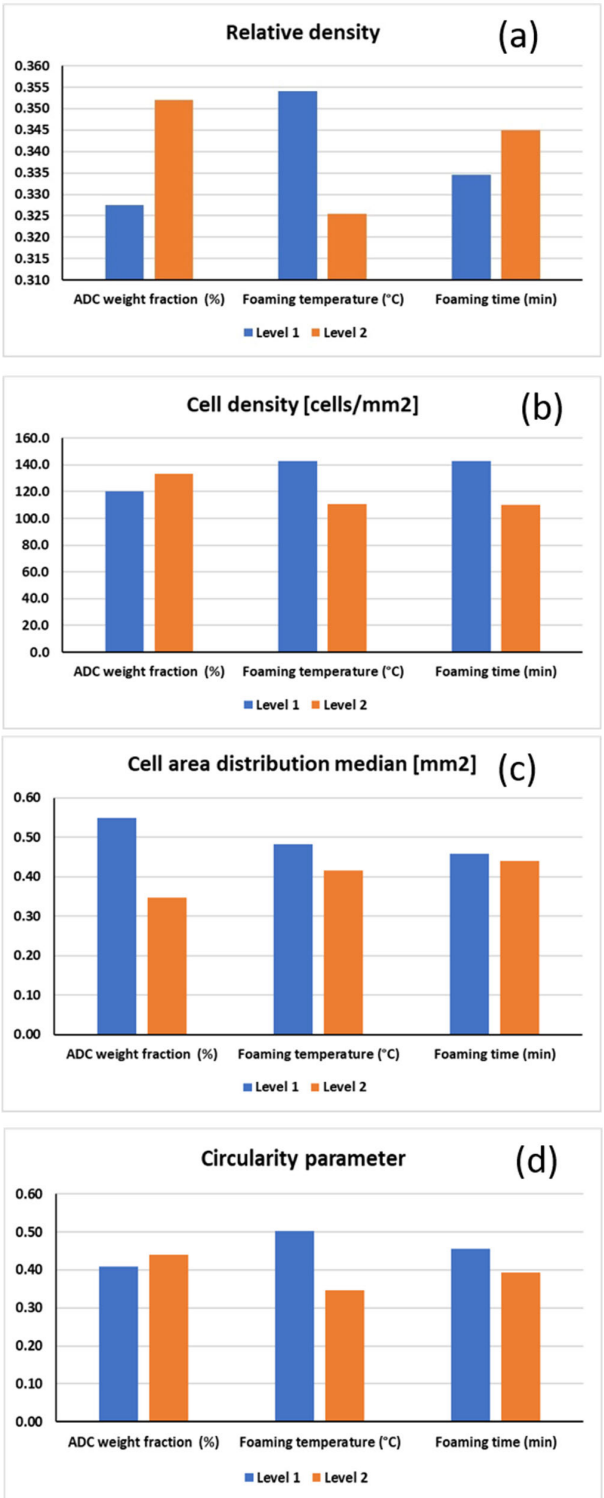

FIGURE 4. (a) Relative Density, (b) Cell density, (c) median of the cell area distribution, and (d) circularity parameter vs. process parameters, ADC wf%, foaming temperature (°C), and time (min) for low (level 1, blue bar) and high (level 2, orange bar) levels.

set by fixing priority targets, as it is not possible to obtain the simultaneous maximization of all morphological indicators.

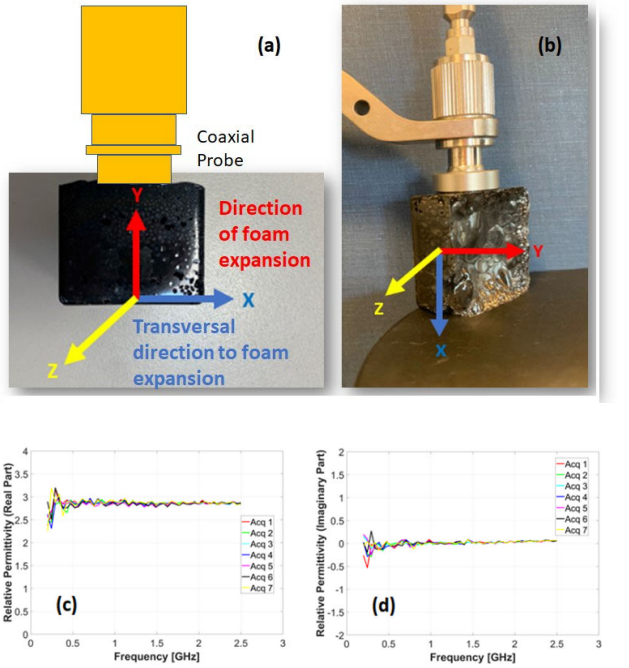

FIGURE 5. (a) PLA foam with acquisition direction; (b) example of complex permittivity acquisition by coaxial probe along the direction transversal to foam expansion. Complex Permittivity measurements of foam sample 1, process parameters: ADC 2 %, T = 190 °C, t = 90 min; (c) 7 acquisitions for the real part of permittivity; (d) 7 acquisitions for the imaginary part of permittivity.

B. MEASUREMENTS OF RELATIVE COMPLEX PERMITTIVITY

The coaxial probe method was used to characterize the foams' relative complex permittivity ε. The measurement setup involved a Coaxial Probe 85070C connected to a Vector Network Analyzer (VNA - Agilent Technologies, 8714ET) operating between 0-2.5 GHz. The method provided the real part ε' and the imaginary part ε''. To evaluate the foam anisotropy, the measurements were performed along two directions, i.e., the foam expansion direction (Y) and the transversal one (X) (Fig. 5a), and repeated seven times each. Figures 5c-d report all plots of real and imaginary permittivity measurements of sample 1 (ADC 1%, T = 190 °C, t = 90 min), which exhibit relevant repeatability.

Fig. 6 depicts the plots referring to the average complex permittivity of sample 2 (Fig. 6a-b) and sample 8 (Fig. 6c-d); for the average curves, a fitting filter was applied to the raw data to cleanse the ripples due to noise. Samples 2 and 8 are chosen once again as they display similar volume and relative density (18.301 mm^3 and 0.338 for sample 2, and 18.352 mm^3 and 0.335 for sample 8) but very diverse cell density, area, distribution, and circularity (see Table 3). In particular, since sample 2 has air cells with larger areas, a lower ε' than sample 8 is expected along the foaming expansion direction, as confirmed by the plots in Fig. 6a,c. Conversely, ε' is higher along the transversal one for both samples. In these cases, higher ε' may be ascribed to a

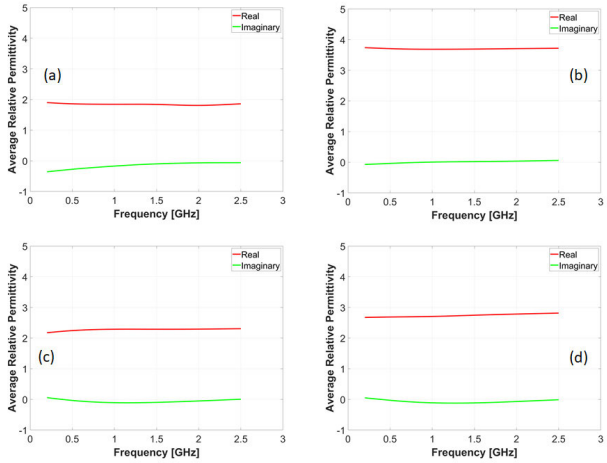

FIGURE 6. Figure 6: Average relative permittivity plots of sample 2 (ADC 1 %, T = 190 °C, t = 120 min): (a) real (red) and imaginary (green) parts along foaming expansion direction-(b) real (red) and imaginary (green) parts along transversal direction; Average relative permittivity plots of sample 8 (ADC 2 %, T = 210 °C, t = 120 min): (c) real (red) and imaginary (green) parts along foaming expansion direction–(d) real (red) and imaginary (green) parts along transversal direction.

more dense non-foamed polymer layer the probe surface was in close contact with. For the analyzed samples, ε'' shows minimal and relatively constant values (0.001-0.02) throughout the frequency range of interest, independently of the acquisition direction. For completeness, all average ε' and ε'' values of all foam samples are summarized in Table 4.

TABLE 4. Average Complex permittivity of all foam samples for foaming and transversal directions.

Sample n.	Average ε' Foaming direction	Average ε' Transversal direction	Average ε'' Foaming direction	Average ε'' Transversal direction
1	2.003	2.496	0.075	0.509
2	1.859	3.720	-0.052	0.059
3	2.929	3.971	0.203	0.052
4	4.332	2.979	5.103	0.063
5	1.513	2.451	0.103	0.086
6	1.824	3.559	-0.452	-0.159
7	1.757	2.681	-0.722	-0.043
8	2.312	2.815	0.005	-0.022

The average values of relative complex permittivity ε, measured in the foaming direction, were also examined in the function of process parameters, ADC%, foaming time, and temperature (Fig. 7 and Fig. 8). As inferred from Fig. 7a-b, ε' generally increases as ADC% and the foaming time are raised while the temperature must be kept as low as possible. These observations also agree with the process settings suggested for obtaining foams with higher relative density and cell density. Similarly to ε', also the imaginary part of the permittivity, ε'' (Fig. 8), tends to increase with ADC% and foaming time, and foaming temperature is more minor.

III. NUMERICAL ANALYSES OF STOCHASTIC AIR CELL DISTRIBUTION MODEL MIMICKING PRODUCED CF-PLA FOAMS

Numerical simulations were performed using the IFDTD method via CST Microwave Studio to predict the behavior of

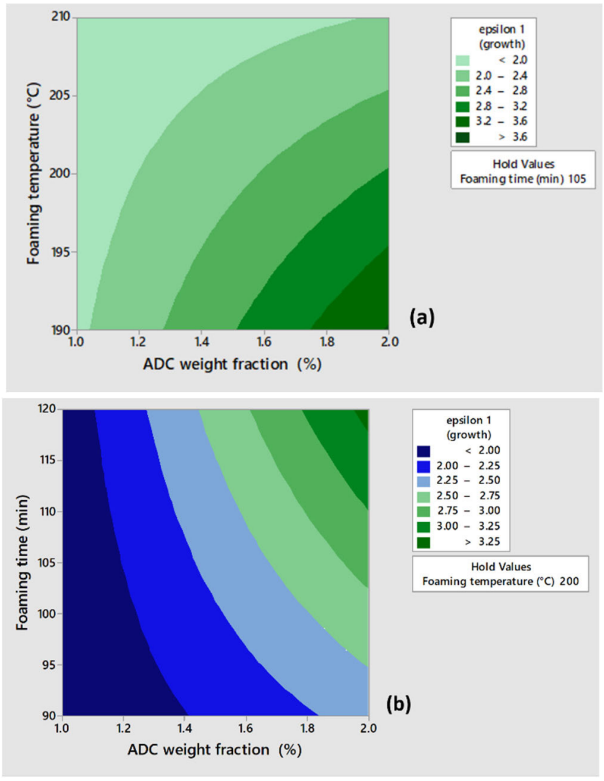

FIGURE 7. Average imaginary permittivity measured along foam expansion direction plotted by varying: a) foaming time and temperature, and b) foaming temperature and ADC weight fraction.

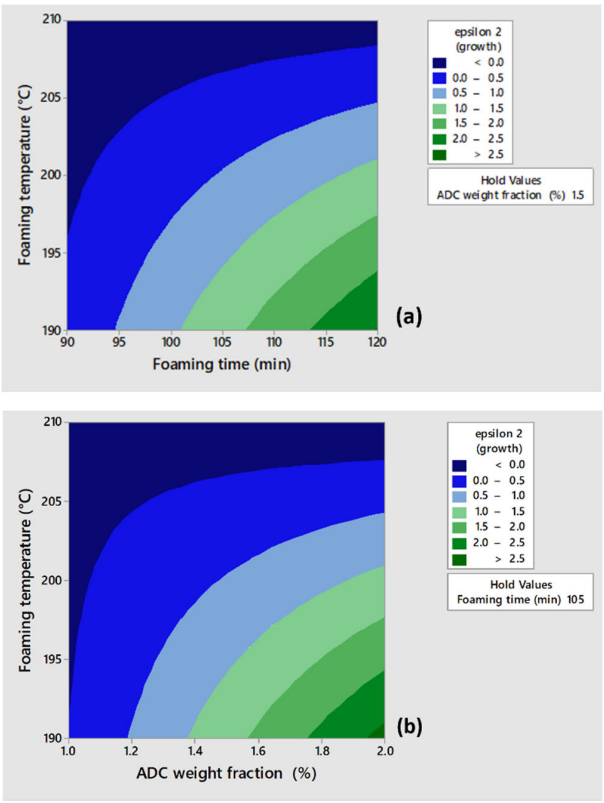

FIGURE 8. Average real permittivity measured along foam expansion direction plotted by varying: a) ADC weight fraction and foaming temperature, b) ADC weight fraction and foaming time.

the CF-PLA foams. The numerical domain (Fig. 9) comprised two air blocks; the incident port 1 and the output port 2 were placed at the beginning of the first air block and the end of the second one, respectively. The excitation was the plane wave propagating along the z direction. The air cells were created within a CF-PLA block by applying a random cell distribution based on the morphological outcomes, with cell dimensions decreasing along z. Perfectly matched layer (PML) boundaries were applied along the propagation direction, while boundaries on the x-y plane were set considering Ex = 0 and Hy = 0.

The CF-PLA permittivity implemented in the numerical analyses was fitted on measurements performed on a 3D-printed block (sizing 50 × 50×30 mm^3) fabricated via fused deposition modeling (FDM), setting 100% infill and honeycomb deposition pattern. The real and imaginary parts of the complex permittivity are depicted in Fig. 10 and are also in excellent agreement with the values reported in the literature [37], [38], [39].

The numerical analyses were computed in the frequency range between 0.5 and 12 GHz to investigate the Scattering parameters, S_{11} and S_{21}, and the SE, as the foam thickness and air pore number vary. The SE contributions have been calculated based on the following formulas (2)-(4) [40],

$$SE = 10\log_{10}\left(\frac{P_i}{P_t}\right) = 10\log_{10}\left|\frac{1}{T}\right| = SE'_R + SE'_A \quad (2)$$

$$SE'_R = 10\log_{10}\left(\frac{P_i}{P_{AV}}\right) = 10\log_{10}\left|\frac{1}{1-R}\right| = 10\log_{10}\left|\frac{1}{1-S_{11}^2}\right|, \quad (3)$$

$$SE'_A = 10\log_{10}\left(\frac{P_{AV}}{P_t}\right) = 10\log_{10}\left|\frac{1-R}{T}\right| = 10\log_{10}\left|\frac{1-S_{11}^2}{S_{21}^2}\right| \quad (4)$$

where Pi and Pt are the total impinging and transmitted power, respectively; Pav is the available power defined as Pi-Pr. SE is the total shielding effectiveness, while SE'$_R$ and SE'$_A$ are the reflective and absorptance contributions to shielding effectiveness, respectively.

Initially, a foam thickness "t" of 15 mm was considered, with a maximum number of randomly distributed air pores equal to N_{pore} = 300, having decreasing dimensions along the propagation direction. It is worth underlining that the air pore number could not be further increased due to the limitations imposed by the finite thickness of the structure, discretization, and calculation burden. Therefore, the relative density of the modeled foam is expected to be higher than those calculated for the samples (Table 2). Indeed, considering the volume of the modeled CF-PLA bulk material (20 × 20×15mm^3), the relative density of the first modeled foam corresponded to 0.75, roughly 2 times higher than all values reported in Table 2. The Scattering parameters depicted in Fig. 11a-b evidence Fabry Perot (FP) resonances

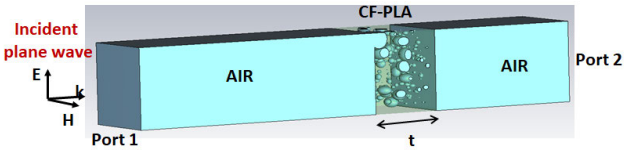

FIGURE 9. Numerical domain of the simulated CF-PLA foam.

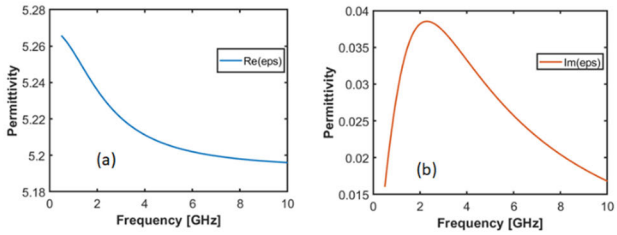

FIGURE 10. (a) real and (b) imaginary permittivity of CF-PLA 3D-printed block.

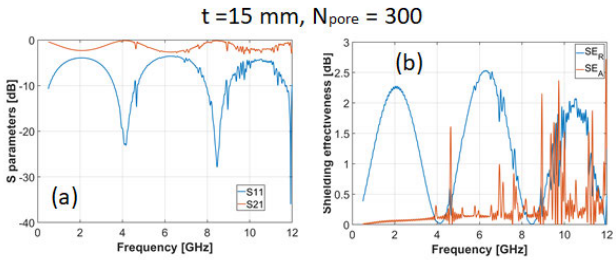

FIGURE 11. (a) Scattering parameters, S_{11} (blue curve) and S_{21} (red curve), and (b) SE_R (blue curve) and SE_A (red curve) of the 15mm thick CF-PLA foam.

typical of a finite dielectric structure at 4.11 GHz and 8.41 GHz.

Nevertheless, S_{11} and S_{21} are simultaneously minimized at 4.65 GHz and 8.95 GHz, where smaller and sharper dips superimpose FP resonances. In order to investigate the resonance types, the electric field modulus at two different frequencies, 4.11 and 4.61 GHz, was inspected. Fig. 12a-b shows that the E-field distribution at 4.11 GHz, outside and inside the modeled foam, is that of an FP resonant mode. In contrast, it can be noticed that at 4.61 GHz (Fig. 12c-d), the E-field modulus is entrapped and enhanced within the air pores, indicating Mie-type resonant mode [41]. Mie-type resonance occurs when a plane wave impinges a dielectric sphere, having a positive refractive index n and diameters approximately equal to λ/n. In such conditions, the E-field confined within the dielectric air pore induces the coupling between the incident wave and the circular displacement current. Therefore, these Mie-type peaks are enrolled for the structure's multiple internal reflection (MIR) mechanism.

Undesirably, the SE components plotted in Fig. 11b show that, although characterized by higher relative density, the modeled foam displays poor shielding capability, as the SE_A and SE_R have comparable maxima of 2.5 dB. This result suggests that the foam's relative density is insufficient to accomplish satisfactory SE, and in particular, SE_A. Hence, additional simulations involving more air pores were performed. However, considering more pore numbers

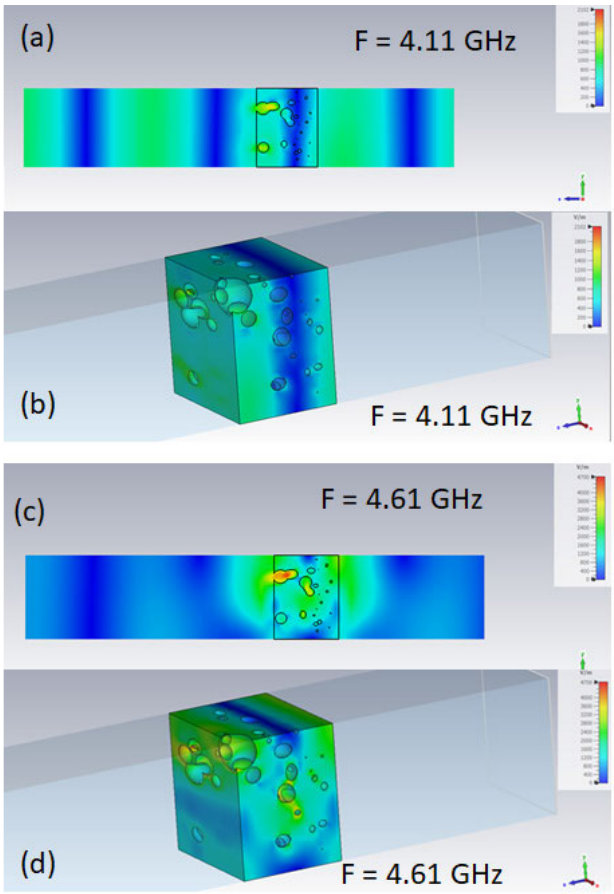

FIGURE 12. (a) E-field module at F = 4.11 GHz, evidencing reflected and transmitted wave due to FP resonance; (b) E-field module describing FP resonant mode inside the foam; (c) E-field module at F = 4.61 GHz, evidencing reflected and transmitted wave due to Mie-like resonance; (b) E-field module describing Mie-like resonant mode inside the foam.

compelled us to simulate also higher foam thicknesses: t = 30 mm and N_{pore} = 500, t = 60 mm, and N_{pore} = 800. Therefore, once again, the relative densities of the modeled foams (Table 5) resulted in higher values than the measured ones. New Scattering parameters, S_{11} and S_{21} (Fig. 13a-c), display an increased number of FP modes, proportional to foam thickness increase. Nonetheless, due to the simultaneous increase of the air pore number, shaper, tighter, and more intense dips referring to Mie-type modes also appear, especially at the higher edge of the frequency range.

Considering the relative density variation of all modeled foams (Table 5), it's reasonable to suppose that the effective relative permittivity of the foamed structures does not vary significantly, which implies a similar impedance mismatch for all case studies. Consequently, SE_R values are expected to be as low as in the previous case, and this trend is confirmed by Fig. 13b and Fig. 13d, which exhibit an SE_R = 2 dB (blue lines). On the contrary, including more air pores with decreasing diameters enhanced the plane wave's coupling with the electric and magnetic dipoles, and consequently

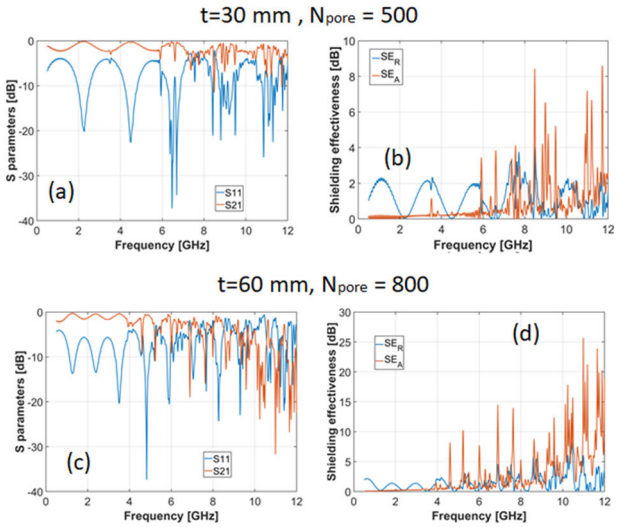

FIGURE 13. (a) Scattering parameters, S_{11} (blue curve) and S_{21} (red curve), and (b) SE_R (blue curve) and SE_A (red curve) of the 30mm thick CF-PLA foam with 500 pores. (c) parameters, S_{11} (blue curve) and S_{21} (red curve), and (d) SE_R (blue curve) and SE_A (red curve) of the 60mm thick CF-PLA foam with 800 pores.

more Mie-type resonances. Hence, the SE_A plots reported in Fig. 13b and Fig. 13d (red lines) pass from values ranging between 1.5-2 dB for N_{pore} = 300 to 8-14 dB for N_{pore} = 800, thus attaining better absorptance.

TABLE 5. Modeled foam thickness and pore number, total volume of the modeled foam, air volume included in the bulk material, and relative density.

Thickness t (mm), Air Pore Number	Total Volume V (mm^3)	Air Volume V_{air} (mm^3)	P = 1-V_{air}/V
15, 300	6000	1513	0.75
30, 500	12000	3407	0.72
60, 800	24000	7990	0.67

IV. SCATTERING PARAMETERS AND SE MEASUREMENTS IN THE X-BAND

The Scattering parameters in the X band were measured for all samples via the setup reported in Fig. 14a-b, comprising a WR90 waveguide connected to the Vector Network Analyzer (VNA - Agilent Technologies, N9917A), operating between 0-18 GHz. The original CF-PLA foams were appropriately cut (Figure 15c) to match the dimensions of the WR90 (22.86 mm x10.16 mm), and their sizes, weight, volume, density, and relative density are reported in Table 6.

As inferable from Table 6, the widths and especially the heights of all cut samples are slightly smaller than the actual sizes of the WR90; however, considering the operating wavelengths in the X-band, the presence of about 1 mm thick air layer is not expected to influence the measurements. The relative density of the samples is reasonably increased compared to the original ones (cf. Table 2 in Section II), as the sample cut was made sacrificing the largest air cells, mainly

TABLE 6. Cut samples' sizes, weight, volume, density, and relative density.

Cut Sample	Width (mm)	Thickness (mm)	$Height_{left}$ (mm)	$Height_{right}$ (mm)	Weight (g)	Volume (cm^3)	Density (g/cm^3)	Relative Density
F1	22.4	17.35	9.5	9.65	1.97	3.721	0.529	0.427
F2	22.5	17.6	9.5	9.1	2.11	3.683	0.573	0.462
F3	22.55	15.9	8.2	8.3	1.82	2.958	0.615	0.496
F4	22.1	16.9	8.8	8.8	2.16	3.287	0.657	0.530
F5	21.22	12.4	8.7	9.5	1.53	2.394	0.639	0.515
F6	22.5	16.15	8	9.15	2.17	3.116	0.696	0.562
F7	22.58	17.2	8.3	7.45	2.38	3.058	0.778	0.628
F8	22.45	15.4	7.5	7.5	2.21	2.593	0.852	0.687

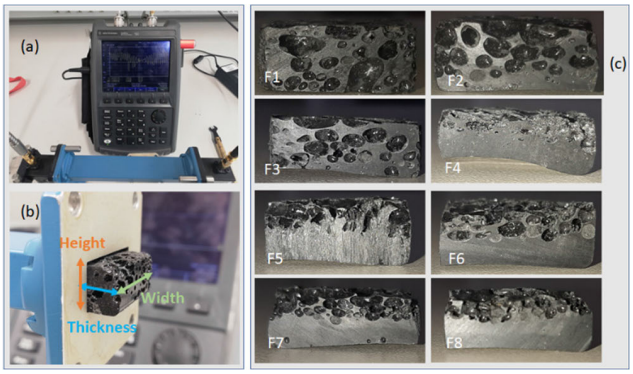

FIGURE 14. (a) Scattering Parameters measurement setup; (b) close-up of the cut foam sample partially inserted in the WR90; (c) foam samples cut for the measurements.

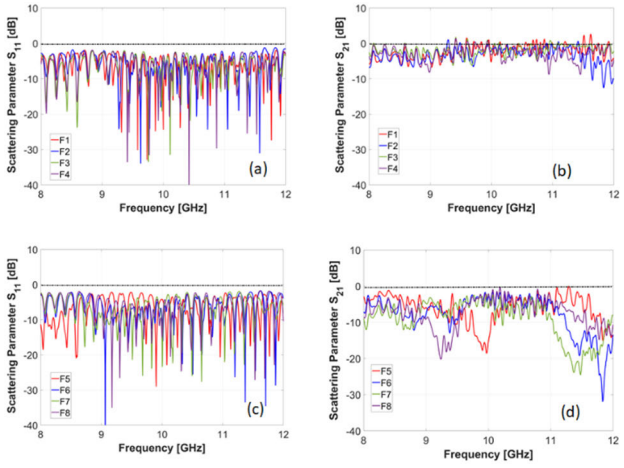

FIGURE 15. Scattering parameters: (a) S_{11} for sample F1 to sample F4; (b) S_{21} for sample F1 to sample F4; (c) S_{11} for sample F5 to sample F8; (d) S_{21} for sample F5 to sample F8.

located at the top of the whole foams. The frequency band considered for this study also justified this choice since the electromagnetic wave interaction would engage smaller air cells rather than larger ones.

Fig. 15 depicts the S_{11} and S_{21} for all cut samples: in particular, S_{11} is quite similar in all measurements, whereas S_{21} exhibits significant differences. Cut samples from F1 to F4 have lower relative densities due to larger air cells, visible in Fig. 14c. Therefore, the S_{21} (Fig.15b) settles around −8 dB in the whole range, except for the F2 and F4 samples, which show minima of −10 dB between 11 and 12 GHz.

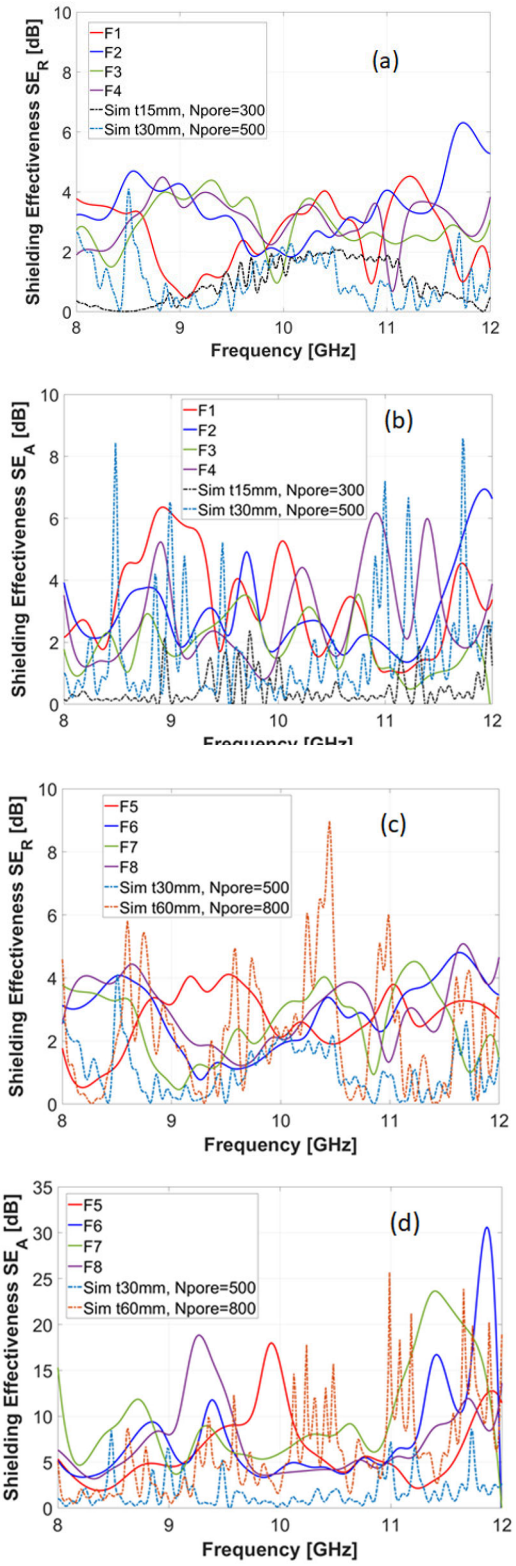

FIGURE 16. (a) SE_R and;(b) SE_A for cut samples from F1 to F4; (c) SE_R and (d) SE_A for cut samples from F5 to F8.

Conversely, the S_{21} trends of cut foams from F5 to F8 (Fig. 15d) display minima around -20 dB down to −30 dB, also covering broader sub-ranges. This result is reasonable

as foams F5, F6, F7, and F8 show higher relative density, ascribed to the presence of tinier air cells and CF-PLA non-foamed substrates (see Fig. 14c).

The SE_R and SE_A (Fig. 16) were then calculated from the Scattering Parameters measurements by using the formulas (2)-(4). A smoothing filter was also applied to the curve representation to increase readability. The dash-dotted lines in Fig. 16 represent the numerical results of the modeled foams. For cut samples from F1 to F4, we considered two specific simulated cases for references since they have morphological similarities, i.e., thicknesses t = 15, 30 mm and N_{pore} = 300, 500. For cut samples from F5 to F8, modeled foams having thicknesses t = 30, 60 mm, and N_{pore} = 500, 800 were plotted; more importantly, the relative densities of these latest modeled cases are closer to those displayed by cut sample F8 (0.687). With such assumptions in mind, it can be noticed from Fig. 16a-b that SE_R and SE_A trends, indicated by the black and light blue-dotted lines, follow the behavior of samples F1 and F2 (solid red and blue-line in Fig.16a-b). In particular, SE_R-measured average values are around 2 dB, whereas SE_A average values and maxima barely reach 4 dB and 6 dB, respectively.

As inferred from Fig. 16c, referring to cut samples from F5 to F8, the SE_R-measured average value equals 3 dB, and the curve trends also appear in good agreement with numerical results (light blue dash-dotted line). Notwithstanding, simulated SE_R related to t = 60 mm and N_{pore} = 800 is higher than the measured SE_R values due to the increased effective relative permittivity ascribed to the larger foam thickness.

Similarly, the SE_A plots depicted in Fig.16d show good agreement with numerical outcomes and remarkable shielding effectiveness due to absorptance; in particular, an average SE_A of 15 dB throughout the X-band and maxima up to 30 dB are obtained. Additionally, each cut sample can shield specific ranges, hinting at the opportunity to accomplish wideband absorption characteristics by properly composing panels with foam samples displaying different relative densities and air pore densities.

V. CONCLUSION

The chemical foaming process was investigated for manufacturing CF-PLA porous structures intended as EMI shields in the X-band. The two-level full factorial design of experiments was performed to realize 8 foamed samples. Their morphological and electromagnetic characterization allowed us to identify the role of the process parameters on the final geometries and dielectric characteristics. In particular, results showed that increasing the blowing agent weight fraction percentage and decreasing the temperature can yield higher foams' relative and air cell densities. The coaxial probe method measurements showed that CF-PLA foams with higher relative and air cell densities generally have higher ε', and this value also differs depending on the acquisition direction due to the relevant structure anisotropy. On the contrary, dielectric losses were low ($\varepsilon'' = 0.007$-0.07), independently of the foam morphological indicators.

Numerical analyses of foams modeled on actual morphological air cell distribution were then performed via CST Microwave Studio to investigate Scattering parameters and EMI SE. The results evidenced that the shielding contribution due to absorption, SE_A, and the one due to reflection SE_R are about 15 dB and 2 dB, respectively. Nonetheless, due to the increased thickness of the models, it was also noticed that the simulated cases featured doubled relative density compared to the fabricated samples. Scattering parameters (S_{11} and S_{21}) and SE were subsequently measured in the X-band using a WR90 waveguide connected with two ports to a VNA. In order to proceed with the measurements, the original foam samples were appropriately cut to match the sizes of the WR90. Considering the frequency range of interest, the foam size adjustment was made by sacrificing larger air cells; consequently, the cut foam's relative densities displayed higher values aligned with the numerical models. The inspection of S_{11} and S_{21} revealed that only samples with higher relative and air cell densities simultaneously provide reduced reflection and transmission. Accordingly, the calculated SE_R and SE_A show that shielding by reflection was minimized (SE_R = 3 dB), whereas shielding by absorption was satisfactory (average SE_A = 15dB in the whole X-band, with maxima up to 30dB). It is also worth underlining that some samples could shield broader sub-ranges; therefore, such foams can be used to compose EMI-shielding panels featuring wideband absorption characteristics.

ACKNOWLEDGMENT

The authors would like to thank Dr. Trunal Patil and Eng. Vito Basile from CNR STIIMA for their support in the technological aspects of the research. *(Valeria Marrocco and Rossella Surace are co-first authors.)*

REFERENCES

[1] V. Marrocco, V. Basile, I. Marasco, G. Niro, L. Melchiorre, A. D'Orazio, M. Grande, and I. Fassi, "Rapid prototyping of bio-inspired dielectric resonator antennas for sub-6 GHz applications," *Micromachines*, vol. 12, no. 9, p. 1046, Aug. 2021, doi: 10.3390/mi12091046.

[2] V. Basile, M. Grande, V. Marrocco, D. Laneve, S. Petrignani, F. Prudenzano, and I. Fassi, "Design and manufacturing of super-shaped dielectric resonator antennas for 5G applications using stereolithography," *IEEE Access*, vol. 8, pp. 82929–82937, 2020, doi: 10.1109/ACCESS.2020.2991358.

[3] D. Wanasinghe and F. Aslani, "A review on recent advancement of electromagnetic interference shielding novel metallic materials and processes," *Compos. B, Eng.*, vol. 176, Nov. 2019, Art. no. 107207, doi: 10.1016/j.compositesb.2019.107207.

[4] E. Mikinka and M. Siwak, "Recent advances in electromagnetic interference shielding properties of carbon-fibre-reinforced polymer composites—A topical review," *J. Mater. Sci., Mater. Electron.*, vol. 32, no. 20, pp. 24585–24643, Oct. 2021, doi: 10.1007/s10854-021-06900-8.

[5] R. Surace, S. Bruno, L. A. C. De Filippis, and A. D. Ludovico, "Multi-objective optimization of aluminium foam manufacturing parameters," *Int. J. Simul. Model.*, vol. 8, no. 2, pp. 81–89, 2009.

[6] A. K. Singh, A. Shishkin, T. Koppel, and N. Gupta, "A review of porous lightweight composite materials for electromagnetic interference shielding," *Compos. B, Eng.*, vol. 149, pp. 188–197, Sep. 2018, doi: 10.1016/j.compositesb.2018.05.027.

[7] M. Wang, X.-H. Tang, J.-H. Cai, H. Wu, J.-B. Shen, and S.-Y. Guo, "Construction, mechanism and prospective of conductive polymer composites with multiple interfaces for electromagnetic interference shielding: A review," *Carbon*, vol. 177, pp. 377–402, Jun. 2021, doi: 10.1016/j.carbon.2021.02.047.

[8] R. Ram, M. Rahaman, and D. Khastgir, "Electromagnetic interference (EMI) shielding effectiveness (SE) of polymer-carbon composite," in *Carbon-Containing Polymer Composites*, M. Rahaman, D. Khastgir, and A. Aldalbahi, Eds. Singapore, Springer, 2019.

[9] J. Yang, X. Liao, J. Li, G. He, Y. Zhang, W. Tang, G. Wang, and G. Li, "Light-weight and flexible silicone rubber/MWCNTs/Fe_3O_4 nanocomposite foams for efficient electromagnetic interference shielding and microwave absorption," *Compos. Sci. Technol.*, vol. 181, Sep. 2019, Art. no. 107670, doi: 10.1016/j.compscitech.2019.05.027.

[10] Y.-Y. Wang, Z.-H. Zhou, C.-G. Zhou, W.-J. Sun, J.-F. Gao, K. Dai, D.-X. Yan, and Z.-M. Li, "Lightweight and robust carbon nanotube/polyimide foam for efficient and heat-resistant electromagnetic interference shielding and microwave absorption," *ACS Appl. Mater. Interface*, vol. 12, no. 7, pp. 8704–8712, Feb. 2020, doi: 10.1021/acsami.9b21048.

[11] B. Zhao, J. Deng, C. Zhao, C. Wang, Y. G. Chen, M. Hamidinejad, R. Li, and C. B. Park, "Achieving wideband microwave absorption properties in PVDF nanocomposite foams with an ultra-low MWCNT content by introducing a microcellular structure," *J. Mater. Chem. C*, vol. 8, no. 1, pp. 58–70, 2020.

[12] A. Bongiorno, C. Pagano, F. Baldi, V. Bellantone, R. Surace, and I. Fassi, "Micro-injection molding of CNT nanocomposites obtained via compounding process," *Polym. Compos.*, vol. 38, no. 2, pp. 349–362, Feb. 2017, doi: 10.1002/pc.23593.

[13] R. Kumar, D. P. Mondal, A. Chaudhary, M. Shafeeq, and S. Kumari, "Excellent EMI shielding performance and thermal insulating properties in lightweight, multifunctional carbon-cenosphere composite foams," *Compos. A, Appl. Sci. Manuf.*, vol. 112, pp. 475–484, Sep. 2018, doi: 10.1016/j.compositesa.2018.07.003.

[14] X. Ma, B. Shen, L. Zhang, Y. Liu, W. Zhai, and W. Zheng, "Porous superhydrophobic polymer/carbon composites for lightweight and self-cleaning EMI shielding application," *Compos. Sci. Technol.*, vol. 158, pp. 86–93, Apr. 2018, doi: 10.1016/j.compscitech.2018.02.006.

[15] M. Antunes, "Recent trends in polymeric foams and porous structures for electromagnetic interference shielding applications," *Polymers*, vol. 16, no. 2, p. 195, Jan. 2024, doi: 10.3390/polym16020195.

[16] Y. Jin, N. Xia, and R. A. Gerhardt, "Enhanced dielectric properties of polymer matrix composites with $BaTiO_3$ and MWCNT hybrid fillers using simple phase separation," *Nano Energy*, vol. 30, pp. 407–416, Dec. 2016.

[17] J. R. Potts, D. R. Dreyer, C. W. Bielawski, and R. S. Ruoff, "Graphene-based polymer nanocomposites," *Polymer*, vol. 52, no. 1, pp. 5–25, 2011.

[18] A. Bregman, E. Michielssen, and A. Taub, "Comparison of experimental and modeled EMI shielding properties of periodic porous xGNP/PLA composites," *Polymers*, vol. 11, no. 8, p. 1233, Jul. 2019, doi: 10.3390/polym11081233.

[19] S. Shi, M. Dai, X. Tao, F. Wu, J. Sun, and Y. Chen, "3D printed polylactic acid/graphene nanocomposites with tailored multifunctionality towards superior thermal management and high-efficient electromagnetic interference shielding," *Chem. Eng. J.*, vol. 450, Dec. 2022, Art. no. 138248.

[20] Q. Lv, X. Tao, S. Shi, Y. Li, and N. Chen, "From materials to components: 3D-printed architected honeycombs toward high-performance and tunable electromagnetic interference shielding," *Compos. B, Eng.*, vol. 230, Feb. 2022, Art. no. 109500.

[21] V. Laur, A. Maalouf, A. Chevalier, and F. Comblet, "Three-dimensional printing of honeycomb microwave absorbers: Feasibility and innovative multiscale topologies," *IEEE Trans. Electromagn. Compat.*, vol. 63, no. 2, pp. 390–397, Apr. 2021, doi: 10.1109/TEMC.2020.3006328.

[22] S. Zhang, C. C. Njoku, W. G. Whittow, and J. C. Vardaxoglou, "Novel 3D printed synthetic dielectric substrates," *Microw. Opt. Technol. Lett.*, vol. 57, no. 10, pp. 2344–2346, Oct. 2015.

[23] D. P. Schmitz, B. G. Soares, G. M. O. Barra, and L. Santana, "Sandwich structures based on fused filament fabrication 3D-printed polylactic acid honeycomb and poly(vinylidene fluoride) nanocomposites for microwave absorbing applications," *Polym. Compos.*, vol. 44, no. 4, pp. 2250–2261, Apr. 2023, doi: 10.1002/pc.27240.

[24] M. Antunes and J. I. Velasco, "Multifunctional polymer foams with carbon nanoparticles," *Prog. Polym. Sci.*, vol. 39, no. 3, pp. 486–509, Mar. 2014.

[25] G. Wu, P. Xie, H. Yang, K. Dang, Y. Xu, M. Sain, L.-S. Turng, and W. Yang, "A review of thermoplastic polymer foams for functional applications," *J. Mater. Sci.*, vol. 56, no. 20, pp. 11579–11604, Jul. 2021.

[26] T. Standau, C. Zhao, S. M. Castellón, C. Bonten, and V. Altstädt, "Chemical modification and foam processing of polylactide (PLA)," *Polymers*, vol. 11, no. 2, p. 306, Feb. 2019, doi: 10.3390/polym11020306.

[27] M. Hamidinejad, B. Zhao, A. Zandieh, N. Moghimian, T. Filleter, and C. B. Park, "Enhanced electrical and electromagnetic interference shielding properties of polymer–graphene nanoplatelet composites fabricated via supercritical-fluid treatment and physical foaming," *ACS Appl. Mater. Interfaces*, vol. 10, no. 36, pp. 30752–30761, 2018.

[28] W. Liu, X. Wu, C. Zhang, and S. Jia, "A facile and clean strategy to manufacture functional polylactic acid bead foams," *Mater. Today*, vol. 36, Aug. 2023, Art. no. 106828.

[29] G. Wang, G. Zhao, S. Wang, L. Zhang, and C. B. Park, "Injection-molded microcellular PLA/graphite nanocomposites with dramatically enhanced mechanical and electrical properties for ultra-efficient EMI shielding applications," *J. Mater. Chem. C*, vol. 6, no. 25, pp. 6847–6859, 2018.

[30] G. Wang, L. Wang, L. H. Mark, V. Shaayegan, G. Wang, H. Li, G. Zhao, and C. B. Park, "Ultralow-threshold and lightweight biodegradable porous PLA/MWCNT with segregated conductive networks for high-performance thermal insulation and electromagnetic interference shielding applications," *ACS Appl. Mater. Interfaces*, vol. 10, no. 1, pp. 1195–1203, 2018.

[31] S. Frackowiak, J. Ludwiczak, K. Leluk, K. Orzechowski, and M. Kozlowski, "Foamed poly(lactic acid) composites with carbonaceous fillers for electromagnetic shielding," *Mater. Des.*, vol. 65, pp. 749–756, Jan. 2015.

[32] *ProtoPasta Carbon Fiber PLA*. [Online]. Available: https://protopasta.com/products/carbon-fiber-pla

[33] L. M. Matuana, O. Faruk, and C. A. Diaz, "Cell morphology of extrusion foamed poly(lactic acid) using endothermic chemical foaming agent," *Bioresource Technol.*, vol. 100, no. 23, pp. 5947–5954, Dec. 2009, doi: 10.1016/j.biortech.2009.06.063.

[34] M. Lustig, Q. Feng, Y. Payan, A. Gefen, and D. Benayahu, "Noninvasive continuous monitoring of adipocyte differentiation: From macro to micro scales," *Microsc. Microanalysis*, vol. 25, no. 1, pp. 119–128, Feb. 2019, doi: 10.1017/s1431927618015520.

[35] J. R. Taylor, "An introduction to error analysis: The study of uncertainties," in *Physical Measurements*. Melville, NY, USA: Univ. Science Books, 1997.

[36] R. Banerjee and S. S. Ray, "Foamability and special applications of microcellular thermoplastic polymers: A review on recent advances and future direction," *Macromolecular Mater. Eng.*, vol. 305, no. 10, p. 10, Oct. 2020, doi: 10.1002/mame.202000366.

[37] G. Boussatour, P.-Y. Cresson, B. Genestie, N. Joly, and T. Lasri, "Dielectric characterization of polylactic acid substrate in the frequency band 0.5–67 GHz," *IEEE Microw. Wireless Compon. Lett.*, vol. 28, no. 5, pp. 374–376, May 2018, doi: 10.1109/LMWC.2018.2812642.

[38] E. Huber, M. Mirzaee, J. Bjorgaard, M. Hoyack, S. Noghanian, and I. Chang, "Dielectric property measurement of PLA," in *Proc. IEEE Int. Conf. Electro Inf. Technol. (EIT)*, Grand Forks, ND, USA, May 2016, pp. 0788–0792.

[39] H.-N. Morales-Lovera, J.-L. Olvera-Cervantes, A. Corona-Chavez, and T. K. Kataria, "Dielectric characterization of anisotropic 3D-printed biodegradable substrates based on polylactic acid [application notes]," *IEEE Microw. Mag.*, vol. 22, no. 9, pp. 18–100, Sep. 2021, doi: 10.1109/MMM.2021.3086336.

[40] M. Peng and F. Qin, "Clarification of basic concepts for electromagnetic interference shielding effectiveness," *J. Appl. Phys.*, vol. 130, no. 22, Dec. 2021, Art. no. 225108, doi: 10.1063/5.0075019.

[41] J. Chen, G. Song, S. Cong, and Z. Zhao, "Resonant-cavity-enhanced electrochromic materials and devices," *Adv. Mater.*, vol. 35, no. 47, Nov. 2023, Art. no. 2300179, doi: 10.1002/adma.202300179.

VALERIA MARROCCO received the M.Sc. degree in electronic engineering and the Ph.D. degree in electromagnetism from the Polytechnic University of Bari, Italy, in 2003 and 2007, respectively. Since 2007, she has been a Research Fellow and a Postdoctoral Researcher with the Polytechnic University of Bari, focusing on designing photonic, metamaterial, and plasmonic devices. She was a Lecturer Assistant of several courses in electronic engineering and a Student Supervisor. In 2011, she joined CNR-ITIA (now CNR-STIIMA), as a Research Fellow and is currently a full-time Researcher. Her research interests include concern micro-manufacturing micro-components and devices, in particular, via micro-EDM technology. She also developed monitoring and modeling techniques for such a technology. Her multidisciplinary research interests are conveyed mainly by designing and fabricating 5G antennas and mm-wave devices with additive manufacturing technologies and investigating related electromagnetic interference solutions in the microwave range.

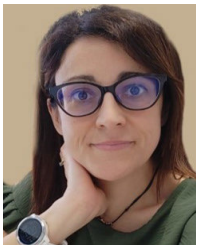

ROSSELLA SURACE received the M.S. degree in mechanical engineering and the Ph.D. degree in advanced production systems from the Polytechnic University of Bari, Bari, Italy, in 2002 and 2007, respectively. In 2005, she was a Visiting Researcher with the Technical University of Helsinki, Helsinki, and the University of Nottingham, Nottingham, U.K., in 2010, where she was with the Manufacturing Division, Precision Manufacturing Centre. Before joining the Institute of Intelligent Industrial Technologies and Systems for Advanced Manufacturing (STIIMA), National Research Council of Italy (CNR), in 2010, she was a Postdoctoral Researcher with the Polytechnic University of Bari. Her research interests include polymer processing technologies (particularly micro-injection molding and additive manufacturing), materials (nanocomposites, recycled polymers, foams), and the material/process/product interlinks.

GIOVANNA CALÒ (Member, IEEE) received the master's degree in electronic engineering and the Ph.D. degree in electromagnetism from the Polytechnic University of Bari, Bari, Italy, in 2002 and 2006, respectively. She joined the Department of Electrical and Electronic Engineering, Polytechnic University of Bari, in 2002, and is currently an Associate Professor of electromagnetism. Her research interests include computational electromagnetics, on-chip optical interconnections, integrated plasmonic nano-antennas for wireless on-chip optical communications, photonic crystals, plasmonic nanostructures, and components.

ELISABETTA BRANDONISIO received the bachelor's degree in building engineering and the master's degree in building systems engineering from the Polytechnic University of Bari, Bari, Italy, in 2012 and 2016, respectively. Since then, she committed to a freelance occupation as a Building Engineer, mainly favoring recycled and phase-changing materials (PCM) for building design. Since 2023, she has been a Research Fellow with CNR-STIIMA, where she processes recycled materials, such as polymers and metals, through foaming and micro-injection molding.

ILARIA MARASCO received the master's degree (summa cum laude) in telecommunication engineering and the Ph.D. degree from Politecnico di Bari, in October 2019 and in 2022, respectively. Since November 2019, she has been with the NPEG-Laboratory, as the Ph.D. Student in collaboration with Istituto Italiano di Tecnologia (IIT), Arnesano, Italy. Since February 2023, she has been an Assistant Professor of electromagnetic fields with Politecnico di Bari. Her research interests include graphene-based components, electrically small antennas on wearable and biodegradable substrates, fabrication technologies for flexible and compact antennas, and piezoelectric resonators for microwave filters and sensors.

FRANCESCA FILOGRANO received the bachelor's degree in medical systems engineering and the master's degree in medical systems engineering (bioengineering) from the Polytechnic University of Bari, Italy, in 2021 and 2023, respectively, where she is currently pursuing the Ph.D. degree with the Department of Electrical and Information Engineering (DEI). Her main research interests metasurfaces, reconfigurable metasurfaces, and photonic and plasmonic devices for medical applications.

IRENE FASSI received the M.Sc. degree in mechanical engineering and the Ph.D. degree in manufacturing technologies from Politecnico di Milano, 1997 and 2001, respectively. Since 1998, she has been a full-time Researcher with CNR-ITIA (now CNR-STIIMA), where she founded and currently leads the research group MEDIS, performing research activities in the field of micro and meso-scale manufacturing and robotics. She regularly gives seminars and courses in the fields of robotics, precision engineering, and advanced manufacturing systems with the University of Brescia and Politecnico di Milano. She is the Research Director of CNR. She is a member of the Executive Board of SIRI (Italian Robotics and Automation Association), a past member of EB of Italian Association of Manufacturing Technologies (AITeM), and the past President of the ASME/DED Technical Committee on Micro and Nano Manufacturing the International Institution for MicroManufacturing.

Open Access funding provided by 'Consiglio Nazionale delle Ricerche-CARI-CARE-ITALY' within the CRUI CARE Agreement